

Soliton dynamics and Peierls-Nabarro barrier in a discrete molecular chain

Larissa Brizhik and Alexander Eremko
Bogolyubov Institute for Theoretical Physics, 252143 Kyiv, Ukraine

Leonor Cruzeiro-Hansson
Mathematics Department, Heriot-Watt University, Edinburgh EH14 4AS, Scotland, United Kingdom

Yulia Olkhovska
Institute of Programming Systems, 252187 Kyiv, Ukraine
 (Received 3 May 1999)

We investigate the motion of a self-localized quasiparticle in a discrete lattice taking into account the interaction of the quasiparticle with the vibrations of the lattice. Using an original method to control the velocity of solitonlike excitations in a discrete system, the dependence of their velocity, momentum, and energy on the carrying wave vector is analyzed. The velocity of the solitonlike excitations is found to saturate at wave vectors below those predicted by continuum models. This is as found in experimental observations. Also, the properties of the Peierls-Nabarro relief, caused by the lattice discreteness, and pinning of a soliton by this barrier, are studied. The influence of the initial condition on the Peierls-Nabarro barrier and soliton motion is investigated. For low-width solitons, a critical value of the wave vector is needed to overcome the Peierls-Nabarro barrier.

I. INTRODUCTION

In the present paper we investigate the dynamics of an electron, or hole, or vibrational or exciton excitation (for simplicity in what follows we call it “quasiparticle”) in a one-dimensional (1D) discrete molecular lattice, taking into account the interaction of the quasiparticle with the longitudinal displacements of the molecules from their equilibrium positions. In 1973 Davydov¹ pointed out that the self-localized excitations in a one-dimensional lattice possess solitonlike features and their transport properties differ greatly from those in bulk crystals. This idea has attracted a great deal of interest and 1D polaron-type states called “Davydov solitons” have become the subject of intensive investigations (a broad review of this work can be found in Ref. 2).

The self-localized polaron states of a quasiparticle can be described by the model Fröhlich Hamiltonian in the zero-order adiabatic approximation. It implies that the total wave function of the system can be written as the product of quasiparticle and phonon states [Davydov ansatz D2 Ref. 2),

$$|\Psi(t)\rangle = |\Psi_e(t)\rangle |\Psi_{ph}(t)\rangle, \quad (1)$$

where $|\Psi_e(t)\rangle$ describes the state of a quasiparticle and $|\Psi_{ph}\rangle$ describes the renormalization of phonons caused by the electron-phonon coupling. The lattice renormalization depends on the quasiparticle state which, in its turn, is determined by the lattice configuration. The adiabatic approximation coincides with the semiclassical approach and leads to a self-consistent system of nonlinear equations of motions that admit a solution in the form of the bound autolocalized state of a quasiparticle and local distortion of the chain (Davydov soliton or 1D polaron).²⁻⁴ The continuum approximation of these equations up to the second order in the functions admits an exact analytical soliton solution that is characterized by the following general features: (a) the soliton can propagate along a chain with constant velocity without changing

its form and without losing energy; (b) the moving soliton is a stationary state of the system with a given value of the total momentum $P_{sol} \neq 0$; (c) the soliton velocity is less than the sound velocity in a chain, $V < V_a$, and tends to the sound velocity with increasing momentum, i.e., $V \rightarrow V_a$, as $P_{sol} \rightarrow \infty$ (and vice versa); (d) the soliton width l_{sol} decreases with increasing velocity, i.e., $l_{sol} \rightarrow 0$ as $V \rightarrow V_a$.

Numerical calculations^{7,8} confirm the main conclusions of the continuum models. Several calculations of the ground state of a quasiparticle have been done at $P_{sol} = 0$ together with a comparison of the polaron energy and of its envelope shape with those obtained in the continuum approximation.^{2,5,6} Regarding moving solitons, numerical studies have been performed of the space-time evolution of some initial excitations (usually localized at the end of a chain).^{2,7,8} These calculations are also in a good agreement with the analytical analysis in the continuum approximation.^{2,7-11} It was shown that some particular initial conditions lead to the formation of soliton(s) moving along a chain. In most cases the initial states are far from the stationary one and launching soliton(s) is usually accompanied by the creation of additional excitations in the form of sound waves and soliton tails. In such approaches, although the soliton velocity is determined by the given initial conditions, it is difficult to vary it in a controlled manner. Here we suggest another method to investigate the traveling soliton in a discrete molecular-cyclic chain. Using an initial excitation in the form of the ground quasiparticle state ($P_{sol} = 0$) calculated numerically, we adiabatically increase its wave vector and, consequently, increase the soliton velocity.

There is ample experimental evidence for polaronlike states in one-dimensional molecular structures.¹²⁻¹⁵ In particular, polarons and bipolarons are considered to be responsible for the high conductivity of conducting polymers. For example, the acoustic solitary-polaron model^{16,17} describes reasonably well the carriers mobility in polydiacetylene, both

in weak and moderate electric fields. However, this model fails in strong electric fields as it predicts that a saturation of the carriers drift velocity should occur at the sound velocity, whereas experimentally this is observed to take place at remarkably lower values ($\sim 0.7V_a$).¹³ The theoretical prediction was obtained within the continuum model, which can break down at large polaron velocities. For a better approximation it is necessary to study the polaron dynamics in the discrete system as done in Sec. III. In this section we show that taking discreteness into account results in qualitative and quantitative differences with respect to the continuum models that provide a possible explanation for the saturation of the drift velocity in polydiacetylene at velocities less than the sound velocity. The results presented in this work depend on the validity of the adiabatic (or semiclassical) approximation. There are three characteristic energies in the system of a quasiparticle interacting with phonons, namely, (i) the energy bandwidth of a free quasiparticle $4J$, (ii) the characteristic phonon frequency $\hbar\Omega_{ph}$, and (iii) the coupling energy E_b . Depending on the relation between these parameters, the system can possess significantly different physical properties (conductivity, optical spectra, etc.). In the general case the problem is very difficult. When one of these three parameters is small (formally proportional to small parameter ε that tends to zero) three well-defined regimes take place. The case $E_b \rightarrow 0$ corresponds to a weak coupling when a quasiparticle behaves as a quasifree one with slightly renormalized energy and effective mass and with finite mean free path. At $J \rightarrow 0$ a quasiparticle is in the small polaron state, and at $\Omega_{ph} \rightarrow 0$ (the limit of atoms with infinite masses M) it is described in the adiabatic approximation as a large polaron. The three characteristic energies can be replaced by two independent dimensionless parameters, e.g., $g = E_b/J$ as the coupling constant and $\gamma = \hbar\Omega_{ph}/J$ as the nonadiabaticity parameter. Depending on the values of these parameters, various regimes are found to be realized.^{18–20} The adiabatic approximation (1) is valid when the inequality is fulfilled,

$$g_{cr,1} < g < g_{cr,2}, \quad (2)$$

where the values of $g_{cr,i}$, $i=1,2$, depend on the value of the nonadiabaticity parameter γ and $g_{cr,1} \rightarrow 0$ as $\gamma \rightarrow 0$.^{18,19} Several investigations have shown good agreement between exact numerical diagonalization and approximate results in this regime.^{21,22}

II. DAVYDOV SOLITON IN A DISCRETE MOLECULAR CHAIN

The Fröhlich Hamiltonian in the case of a single isolated band of a quasiparticle and one phonon mode reads as

$$H = \sum_k E(k) B_k^\dagger B_k + \frac{1}{\sqrt{N}} \sum_{k,q} \chi(k,q) B_k^\dagger B_{k-q} (b_q + b_{-q}^\dagger) + \sum_q \hbar\Omega_q b_q^\dagger b_q. \quad (3)$$

With the Born–von Karman periodic boundary conditions assumed, the wave numbers take the following values:

$$k = \frac{2\pi l}{Na}, \quad l = 0, \pm 1, \dots, \pm \left(\frac{N}{2} - 1\right), \frac{N}{2}, \quad (4)$$

where N is the number (chosen to be even) of molecules in a chain. The Hamiltonian commutes with the operators of the number of quasiparticles \mathcal{N} and total momentum \mathcal{P} ,

$$\mathcal{N} = \sum_k B_k^\dagger B_k, \quad \mathcal{P} = \sum_k \hbar k B_k^\dagger B_k + \sum_q \hbar q b_q^\dagger b_q. \quad (5)$$

The creation B_k^\dagger and annihilation B_k operators of a quasiparticle with the wave number k are connected with the creation B_n^\dagger and annihilation B_n operators of a quasiparticle on a site n by the unitary transformation,

$$B_n = \frac{1}{\sqrt{N}} \sum_k B_k e^{ikna}. \quad (6)$$

The operators b_q^\dagger, b_q are the Bose operators of phonons with the wave number q and frequency Ω_q that are connected with the operators of the molecule displacements U_n and canonically conjugated momenta P_n by the unitary transformation

$$U_n = \frac{1}{\sqrt{N}} \sum_q \left(\frac{\hbar}{2M\Omega_q} \right)^{1/2} (b_q + b_{-q}^\dagger) e^{iqna},$$

$$P_n = -i \frac{1}{\sqrt{N}} \sum_q \left(\frac{\hbar M\Omega_q}{2} \right)^{1/2} (b_q - b_{-q}^\dagger) e^{iqna}. \quad (7)$$

We assume that the electron-phonon coupling χ satisfies the condition (2) for the applicability of the adiabatic approximation (1). The form of the interaction operator in Eq. (3) indicates that the presence of a quasiparticle causes an oscillator displacement and the renormalized phonon state can be written as

$$|\Psi_{ph}(t)\rangle = S|0\rangle_{ph}, \quad (8)$$

with the unitary operator

$$S = \exp \left[\frac{1}{\sqrt{N}} \sum_q [\beta_q(t) b_q^\dagger - \beta_q^*(t) b_q] \right]. \quad (9)$$

Below we consider one-particle states and the operators B_k and B_n can satisfy any statistics. The important condition is that $B_k|0\rangle = 0$ where $|0\rangle$ is the vector of the ground state. Therefore, the Hamiltonian (3) can represent an electron or hole (B_k are Fermi operators), an intramolecular excitation (B_n are Pauli operators) as well as a high-frequency intramolecular excitation (B_k are Bose operators). The single quasiparticle state can be written in a general form,

$$|\Psi_e(t)\rangle = \sum_k \Psi_k(t) B_k^\dagger |0\rangle_e. \quad (10)$$

The states $|0\rangle_e$ in Eq. (10) and $|0\rangle_{ph}$ in Eq. (8) describe, respectively, the ground states of the molecules (or electron subsystem) and of the phonons in a chain in the absence of an extra quasiparticle.

Substituting the wave function in the zero-order adiabatic approximation (1) with account of Eqs. (8)–(10), into the

Schrödinger equation for the Hamiltonian (3) (Refs. 23–25) or using the semiclassical approach,^{26–28} one can obtain the following system of equations:

$$i\hbar \frac{d\Psi_k}{dt} = [W + E(k)]\Psi_k + \frac{1}{N} \sum_q \chi(k, q) \sqrt{\frac{2M\Omega_q}{\hbar}} Q_q \Psi_{k-q}, \quad (11)$$

$$\frac{d^2 Q_q}{dt^2} = -\Omega_q^2 Q_q + \sum_k \chi(k, q) \sqrt{\frac{2\Omega_q}{M\hbar}} \Psi_{k-q}^* \Psi_k. \quad (12)$$

Here,

$$Q_q = \sqrt{\frac{\hbar}{2M\Omega_q}} (\beta_q + \beta_{-q}^*), \quad (13)$$

and W is the energy of the deformation,

$$W = \frac{M}{2} \sum_q \left(\left| \frac{dQ_q}{dt} \right|^2 + \Omega_q^2 |Q_q|^2 \right). \quad (14)$$

The explicit dependence of functions $E(k)$, Ω_q , and $\chi(k, q)$ on the wave vector is determined by the model under consideration. We use the Davydov model for a chain that includes a short-range interaction of a quasiparticle with acoustical phonons and assume that the quasiparticle energy band is formed by the nearest-neighbors interactions. In this case, we have

$$E(k) = E_0 - 2J \cos ka, \quad \Omega_q = 2 \sqrt{\frac{w}{M}} |\sin(qa/2)|, \\ \chi(k, q) = i\chi \sqrt{\frac{2\hbar}{M\Omega_q}} \sin(qa). \quad (15)$$

Introducing the quasiparticle wave function ψ_n and the displacements U_n of the n th molecule given by the unitary transformation,

$$\psi_n(t) = \frac{1}{\sqrt{N}} \sum_k \Psi_k e^{ikna}, \quad U_n = \frac{1}{\sqrt{N}} \sum_q Q_q e^{iqna}, \quad (16)$$

we can get the following system of equations:

$$i\hbar \frac{\partial \psi_n}{\partial t} = (E_0 + W) \psi_n - J(\psi_{n-1} + \psi_{n+1}) + \chi(U_{n+1} - U_{n-1}) \psi_n, \quad (17)$$

$$M \frac{d^2 U_n}{dt^2} = \chi(|\psi_{n+1}|^2 - |\psi_{n-1}|^2) + w(U_{n+1} + U_{n-1} - 2U_n). \quad (18)$$

The total energy of the system,

$$E = \sum_n [-J\psi_n^*(\psi_{n+1} + \psi_{n-1}) + \chi(U_{n+1} - U_{n-1})|\psi_n|^2 + (E_0 + W)|\psi_n|^2], \quad (19)$$

and the total momentum, determined by the operator (5),

$$\mathcal{P} = \sum_k \hbar k |\psi_k|^2 + iM \sum_q q \frac{dQ_q}{dt} Q_{-q} \quad (20)$$

are constants of motion.

Let us choose the solution of Eqs. (17)–(18) in the following form:²⁹

$$\psi_n(t) = \Phi_n(t) e^{ikna - iEt/\hbar}, \quad (21)$$

where k is a discrete variable, determined in Eq. (4), and $\Phi_n(t)$ is assumed to be a real function of n . Substituting Eq. (21) into Eq. (17) leads to the equations

$$\Lambda \Phi_n - J \cos(ka) (\Phi_{n-1} + \Phi_{n+1}) + \chi(U_{n+1} - U_{n-1}) \Phi_n = 0, \quad (22)$$

$$\frac{d\Phi_n}{dt} = -\frac{J}{\hbar} \sin(ka) (\Phi_{n+1} - \Phi_{n-1}), \quad (23)$$

where $\Lambda = E_0 + W - E$.

From Eq. (23) one gets

$$\Phi_n(t) = \sum_q f_q \exp\{i[qan - vt \sin(qa)]\}, \quad v = V/a, \quad (24)$$

where

$$V = V_g \sin(ka), \quad V_g = \frac{2Ja}{\hbar}. \quad (25)$$

The function (24) describes a traveling wave depending on the variable $n - vt$ only in the long-wave (continuum) approximation when $\sin(qa) \approx qa$. In this case for smooth soliton envelope functions $\Phi_n(t)$ and $U_n(t)$, the continuum approximation of Eqs. (22)–(23) leads to the soliton solution,

$$\Phi_{sol}(x, t) = \sqrt{\frac{\mu a}{2}} \frac{1}{\cosh[\mu(x - Vt)]}. \quad (26)$$

Here the velocity V is connected with k by Eq. (25) and

$$\mu = \frac{G}{a(1-s^2)\cos(ka)}, \quad G = \frac{\chi^2}{Jw}, \quad s^2 = \frac{V_{gr}^2}{V_{ac}^2} \sin^2(ka). \quad (27)$$

The main characteristic of the moving soliton is the wave vector k that determines the soliton velocity and momentum:

$$E_{sol}(k) = E_0 - 2J \cos(ka) - \frac{\chi^4(1-5s^2)}{3Jw^2(1-s^2)^3 \cos(ka)}, \quad (28)$$

$$P_{sol}(k) = \hbar k + \frac{8a\chi^4 \tan(ka)}{3\hbar V_{ac}^2 w^2 (1-s^2)^3}. \quad (29)$$

The functions (21), (24) constitute only a first approximation to a traveling quasiparticle in the discrete system. In the case $V_{gr} \gg V_a$ this approximation coincides with the results

of the continuum models because only small values of k are possible, the velocity is proportional to k and tends to the sound velocity V_a .

In the case of a narrow electron band, for small values of k the velocity also turns out to be proportional to k , as happens in the continuum approximation. At large values of k , the velocity is bounded from above by the group velocity: $V \rightarrow V_{gr}$ at $k \rightarrow \pi/a$.

This solution shows that in the continuum approximation at small values of the soliton velocity V the shape of the traveling soliton is very close to the shape of the soliton at rest, and that its amplitude increases and the width decreases with increasing velocity. At large velocities these changes become significant and the applicability of the continuum approximation is violated, and therefore, the discrete description is necessary. Moreover, Eq. (24) shows that the space-time evolution of the envelope function is more complicated than the one predicted by the continuum approximation with its functional dependence on the variable $n - vt$. Hence, in the discrete system one can expect the manifestation of the Peierls-Nabarro relief^{30,31} in the quasiparticle dynamics. This question is discussed in Sec. IV.

The exact analytical solution of the initial system of discrete Eqs. (17)–(18) is not known and numerical calculations are thus very useful. Unlike the stationary case that has zero velocity, special attention should be paid to the choice of the initial conditions in the numerical study at nonzero velocities. The deviation of the initial condition, even if it is chosen in the form of the continuum solution, from the exact steady state in this latter case is large. This can result in strong emission of phonons that will influence the quasiparticle significantly and the system will remain far from the steady state. One possible way to eliminate this energy excess is to introduce friction. Another way is to try to guess an initial condition very close to the traveling steady state. The analytical analysis above can be used for the proper choice of initial conditions in the numerical study of traveling excitations in discrete systems. At time moment $t=0$ the soliton solution of Eqs. (17)–(18) has the form

$$\psi_n(0) = \Phi_n(0; k) e^{ikna}, \quad U_n(0) = \frac{1}{N} \sum_q U(q, 0; k) e^{iqna},$$

$$\left. \frac{dU}{dt} \right|_{t=0} = -i \frac{2Ja}{N\hbar} \sin(ka) \sum_q q U(q, 0; k) e^{iqna}. \quad (30)$$

At small k according to Eq. (30), one has $\Phi_n(0; k + \delta k) \approx \Phi_n(0; k)$, $U(q, 0; k + \delta k) \approx U(q, 0; k)$. This gives rise to the following choice of the initial conditions for the traveling soliton in the discrete system:

$$\psi_n(0; k + \delta k) = \psi_n(0; k) e^{i\delta kna}, \quad U_n(0; k + \delta k) = U_n(0; k),$$

$$\left. \frac{dU_n(k + \delta k)}{dt} \right|_{t=0} = -\frac{J}{\hbar} [U_{n+1}(0; k) - U_{n-1}(0; k)] \times \sin[(k + \delta k)a]. \quad (31)$$

We start with zero wave vector $k=0$, and choose the functions $\psi_n(t=0; 0)$ and $U_n(t=0; 0)$ in the form obtained by exact numerical minimization of the energy functional (19).⁵

Then we use the relations (31) for small values of the dimensionless wave number δka . Thus, we get the traveling wave solutions with greater velocities by substituting $\psi_n(0; k_m)$ and $U_n(0; k_m)$ by the steady-state solutions obtained previously at some $t=t_0$ for a smaller velocity:

$$\psi_n(t=0, k_{m+1}) = \psi_n(t=t_0, k_m) e^{i\delta kna},$$

$$k_{m+1} = k_m + \delta k, k_0 = 0, \quad (32)$$

with the same molecule displacements and corresponding site velocities according to Eq. (31). In this way we disturb the shape of the pulse slightly and increase the velocity of the pulse in an iterative manner. The validity of this approach and its efficiency are demonstrated by the results of the numerical calculations, as it will be shown below.

In the next section we discuss the results of the numerical integration of the discrete system of Eqs. (17) and (18) with the normalization and periodic boundary conditions

$$\sum_n |\psi_n|^2 = 1, \quad \psi_{n+N} = \psi_n, \quad U_{n+N} = U_n, \quad (33)$$

using Eq. (31) as an initial condition. For this it is useful to rewrite Eqs. (17) and (18) in dimensionless variables:

$$i \frac{\partial \psi_n}{\partial \tau} = E \psi_n - (\psi_{n-1} + \psi_{n+1}) + X(u_{n+1} - u_{n-1}) \psi_n, \quad (34)$$

$$\frac{d^2 u_n}{d\tau^2} = Y(|\psi_{n+1}|^2 - |\psi_{n-1}|^2) + Z(u_{n+1} + u_{n-1} - 2u_n). \quad (35)$$

Here,

$$\tau = \frac{Jt}{\hbar}, \quad u_n = \frac{U_n}{a}, \quad E = \frac{\Lambda}{J},$$

$$X = \frac{a\chi}{J}, \quad Y = \frac{\hbar^2 \chi}{MaJ^2}, \quad Z = \frac{\hbar^2 w}{MJ^2}. \quad (36)$$

III. RESULTS OF NUMERICAL CALCULATIONS

We have performed numerical calculations for a lattice with $N=50$ sites, under periodic boundary conditions in the manner discussed in the previous section. We have chosen numerical values of the parameters that are characteristic of the protein alpha helix and other quasi-one-dimensional polypeptides. Namely,

$$J = 1.55 \times 10^{-22} \text{ J}, \quad w = 39 \text{ N/m}, \quad M = 5.7 \times 10^{-25} \text{ Kg},$$

$$\chi = 62 \times 10^{-12} \text{ N}, \quad a = 4.5 \times 10^{-10} \text{ m}. \quad (37)$$

In some of the calculations these parameters were changed as specified in the text and in the figure captions.

The results of the calculations are reported in the figures. They show that increasing the value of k within a given interval, the amplitude and the velocity of the soliton pulse increases (see Fig. 1, Fig. 2, and Fig. 3). It might be expected that, with increasing k , the current (in the case of transfer of charges) will increase monotonically. Instead, the numerical

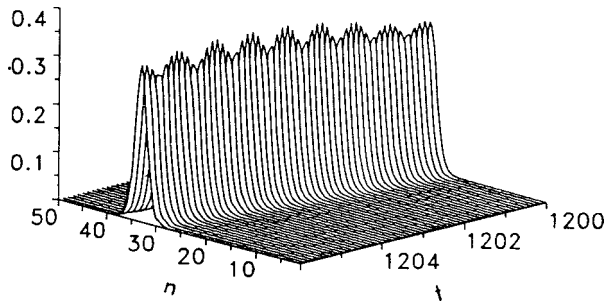


FIG. 1. Amplitude of the soliton envelope as a function of the lattice site n and time t , at $l=1$, ($k=2\pi l/N$).

simulations show that, although this happens for small values of k , with further increases of k a saturation of the soliton velocity at a constant value V_0 takes place. The saturation velocity V_0 and the value of k for which this saturation occurs, depend on the values of the parameters of the chain (see Fig. 4). The maximum soliton velocity when $\chi' = \chi, J' = J, w' = 9.25$ N/m is approximately two-thirds of the sound velocity in the chain, as seen in Fig. 4. This is less than the value predicted by the analysis based on the continuum model. Our results, based on the discrete model, can thus explain the saturation of the drift velocity in the polydiacetylene at velocities less than the sound velocity that was reported in Ref. 17. Moreover, the increase of the soliton velocity results in the perturbation of the soliton, that is, its envelope changes, oscillating tails appear, and their amplitude and energy increase with k . At the same time, the total current in the system, $j = i\hbar \sum_n (\psi_n^* \psi_{n-1} - \psi_{n-1}^* \psi_n)$, first, increases with k , and, for large values of k , it reaches a *plateau*. Further increase of the carrying wave vector k results in the decrease of the current due to the more intensive emission of phonons and radiation from the soliton (compare Fig. 3 and Fig. 5). This corresponds to the region of negative resistance that is observed experimentally at large fields, in some conducting polymers. Also, the transfer of the energy of the initial excitation to delocalized modes that takes place at large values of k , leads to a reduction of the total-energy flux. The conclusion is that the population of delocalized modes absorbs the energy, but they do not contribute to the current in the system.

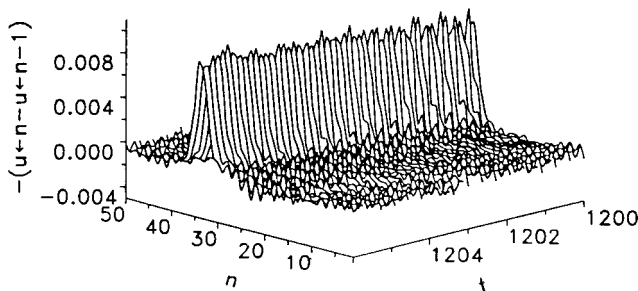


FIG. 2. Chain deformation $u_n - u_{n-1}$ as a function of the lattice site and time at $l=1$.

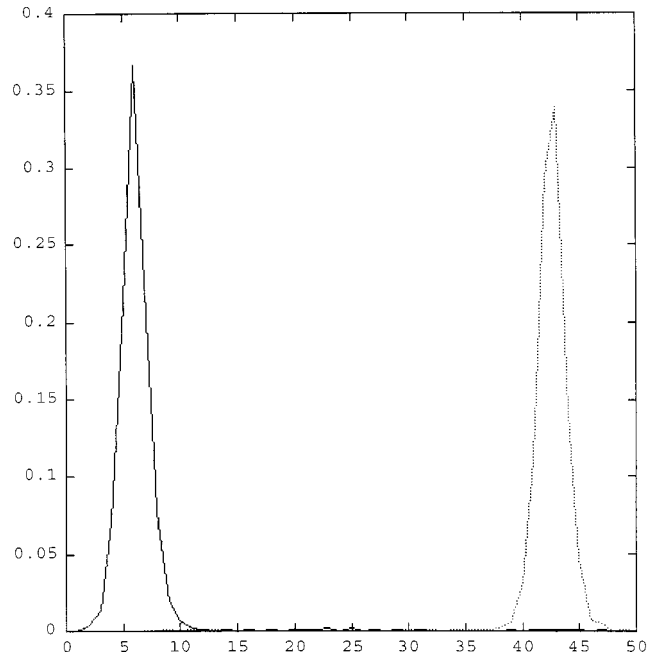


FIG. 3. Amplitude of the soliton envelope as a function of the lattice site n for different times, $\tau=25$ (solid line), and $\tau=175$ (dashed line), at $l=6$.

The average soliton momentum and energy for small values of the velocity, and, correspondingly, for low k , are close to the values predicted by the continuum approximation, being proportional to the first and second power of the velocity, from the continuum results are increasingly apparent as k increases (see Fig. 4).

The effective soliton mass can be obtained from Eq. (29) at small velocities:

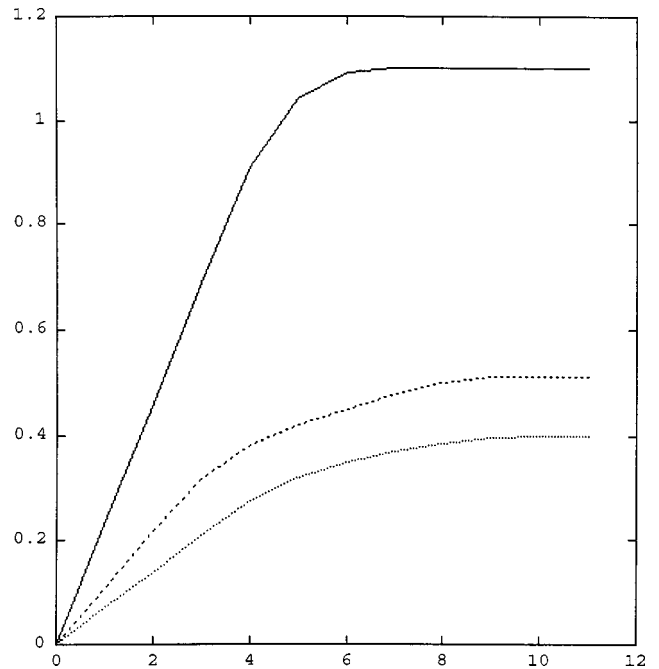


FIG. 4. Dependence of the soliton velocity on the wave number for different sets of parameters. The solid line corresponds to the set of parameters given by Eq. (37); the dotted line corresponds to $\chi' = 2\chi, J' = 4J, w' = w$; and the dashed line corresponds to $\chi' = \chi, J' = J, w' = 9.25$ N/m.

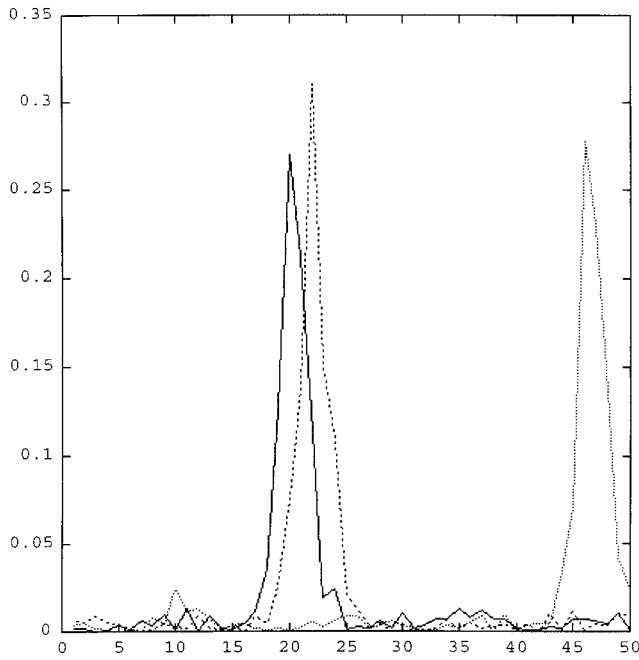


FIG. 5. Amplitude of the soliton envelope as a function of the lattice site n for different times, $\tau=560$ (solid line), 580 (dashed line), and 600 (dotted line) at $l=-10$.

$$m_s = m \left(1 + \frac{8a^2 \chi^4}{3\hbar^2 w^2 V_{ac}^2} \right), \quad m = \frac{\hbar^2}{2Ja^2}. \quad (38)$$

It can also be observed from the numerical calculations

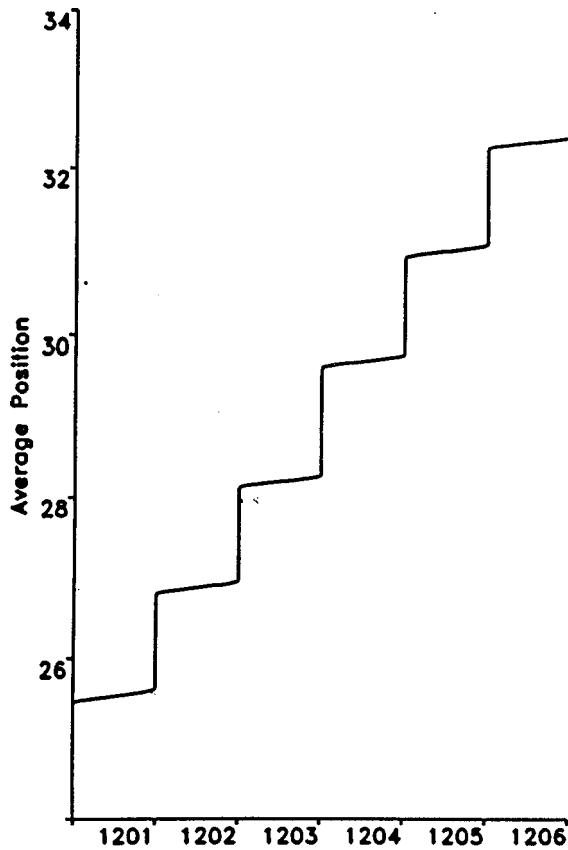


FIG. 6. Soliton c.m.c. as a function of time at short time scale, for $l=10$.

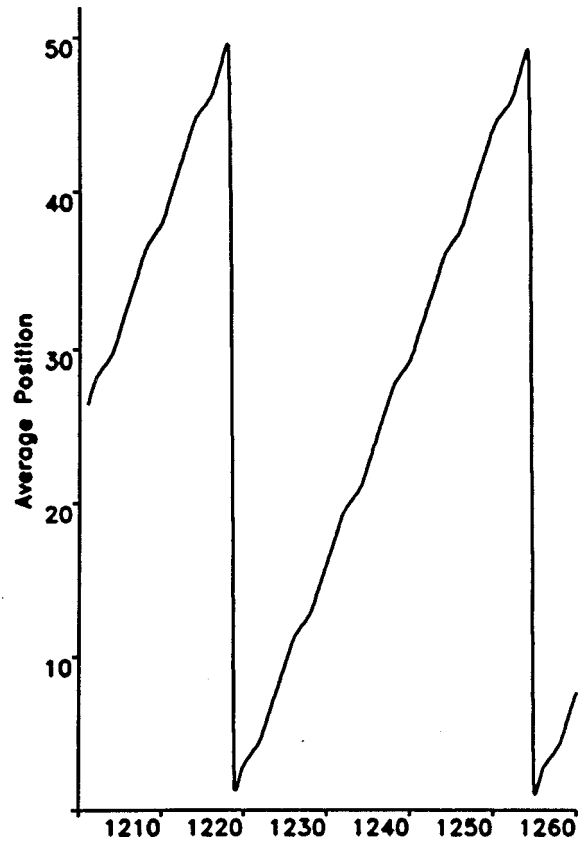


FIG. 7. Soliton c.m.c. as a function of time at large time scale for $l=10$.

that the motion of the localized pulse is discrete, it has the form of discrete jumps from site to site even for rather wide pulses (see Fig. 6). At a large time scale the center of mass coordinate (c.m.c.) of the pulse [see Eq. (20)] is displaced along the chain with constant velocity, as it is shown in Fig. 7. It is also worth mentioning the stability of soliton envelope throughout propagation, which can be seen in Fig. 5 (remember that the figures show soliton pulses that have passed the chain ring many times before reaching the present positions).

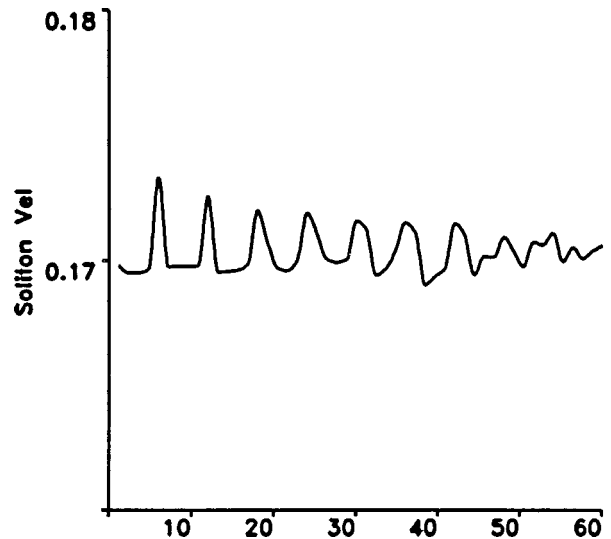


FIG. 8. Soliton velocity for $l=10$.

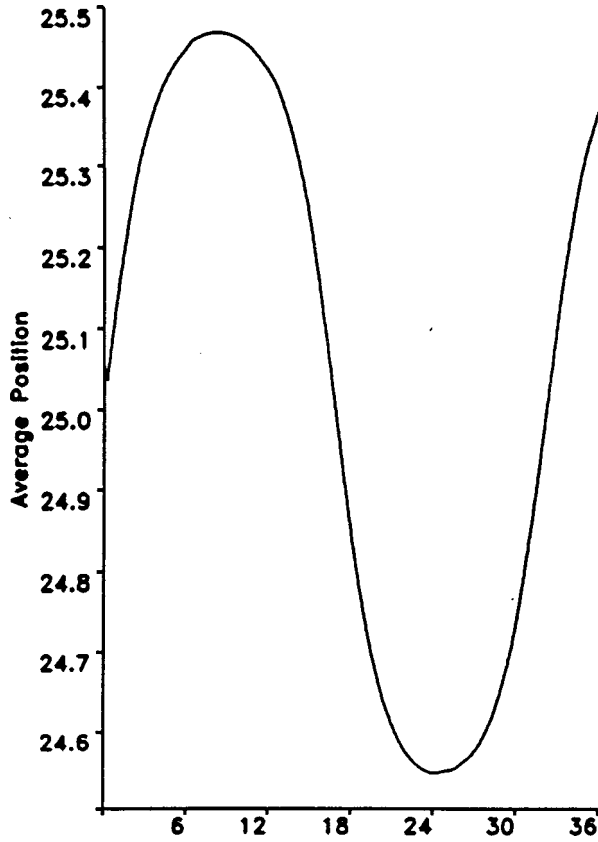


FIG. 9. Soliton c.m.c. as a function of time ($\chi=91$ pN, $l=1$).

IV. PEIERLS-NABARRO BARRIER

The numerical investigations reported in the previous section, demonstrate the manifestation of the lattice discreteness in several ways. The main qualitative difference between the continuum and the discrete model is the periodicity of the latter with the lattice constant a . First of all, in the periodic lattice the quasiparticle energy band has a finite width $4J$ and the energy dispersion differs from the parabolic law at large values of k . This is taken into account by Eq. (21), which results in the relation (25) between the velocity V of soliton wave packet and carrying wave vector k .

Second, the manifestation of the Peierls-Nabarro barrier is clearly apparent in the soliton motion at high time resolution, as is shown in Fig. 6 and Fig. 8. The “instantaneous” soliton velocity depends on time, as would be expected for the motion of a quasiparticle in a periodical potential. The influence of the Peierls-Nabarro relief on Davydov solitons has been shown in Ref. 32 by variational numerical calculations, and in Ref. 33 the periodic relief was studied using the completely integrable discrete Ablowitz-Ladik model.³⁴ The system of coupled Eqs. (17) and (18) that describes molecular solitons (one-dimensional large polarons) does not belong to any completely integrable class, and numerical calculations are very useful to extend and complement continuum models. The proper analytical studies can be fruitful for a better understanding of the results obtained in the previous section. In this section we present such analysis. It takes into account the periodicity of the lattice, not only in the coordinate space, but also in the space of reciprocal lattice vectors. This latter periodicity results in umklapp processes in the interactions

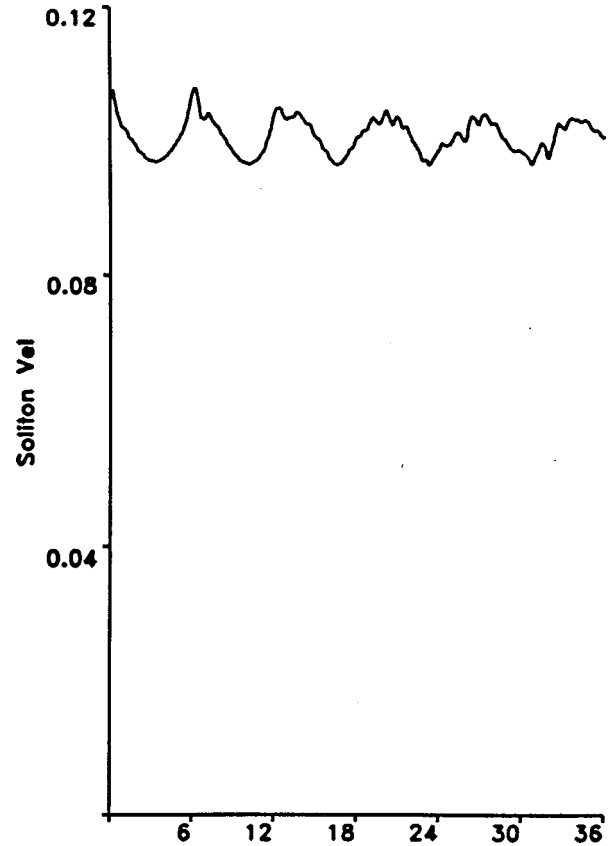


FIG. 10. Soliton velocity as a function of time ($\chi=80$ pN, $l=1$).

between quasiparticles in crystals. In Eqs. (11)–(12) the wave vectors are in the first Brillouin zone, $-\pi/a < k \leq \pi/a$, and one can introduce the summation over wave vectors k' replacing $k-q$ and taking into account the quasimomentum conservation law,

$$\Delta(k-q-k') = \begin{cases} \delta_{k-q,k'} & \text{if } |k-q| \leq \frac{\pi}{a}, \\ \delta_{k-q-g,k'} & \text{if } k-q > \frac{\pi}{a}, \\ \delta_{k-q+g,k'} & \text{if } k-q < -\frac{\pi}{a}, \end{cases}$$

where $g=2\pi/a$ is the vector of a reciprocal lattice. This does not change the discrete Eqs. (17) and (18) because the relation $\Psi_{k\pm g} = \Psi_k$ applies, but it is essential when introducing continuous functions for the analytical investigation of Eqs. (11) and (12) that are equivalent to Eqs. (17) and (18). Let

$$\psi(x,t) = \frac{1}{\sqrt{L}} \sum_k \Psi_k(t) e^{ikx}, \quad u(x,t) = \frac{1}{N} \sum_q Q_q e^{iqx}, \quad (39)$$

where $L=Na$. One can see that these functions are periodical, i.e., $\psi(x+L,t) = \psi(x,t)$ and $u(x+L,t) = u(x,t)$. From Eq. (39) we derive the relation

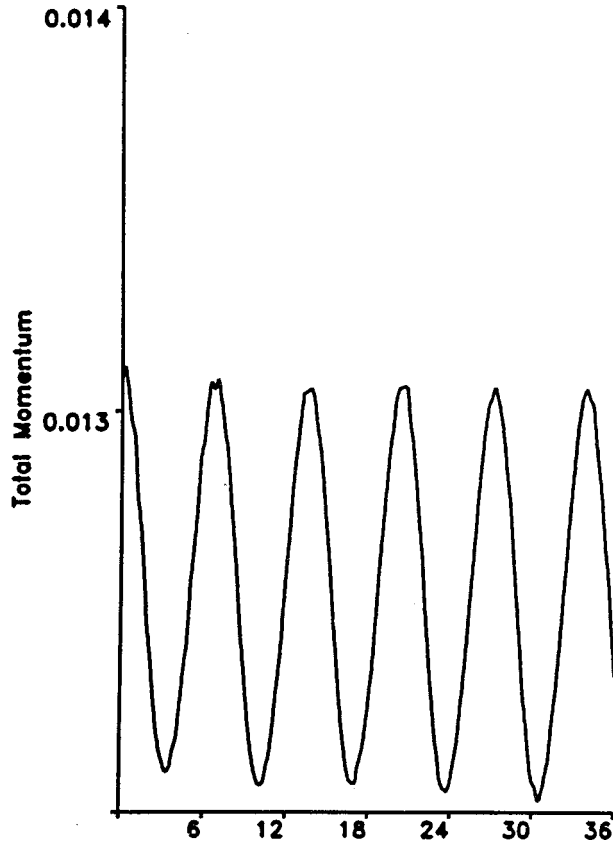


FIG. 11. Soliton momentum as a function of time ($\chi = 80$ pN, $l=1$). The c.m.c. of the soliton is a linear function of time within the same time scale.

$$\Psi_k(t) = \frac{1}{\sqrt{L}} \int_{-L/2}^{L/2} \psi(x,t) e^{-ikx} dx \quad (40)$$

in the continuum approximation. We assume that in the k representation the soliton wave packet is narrow and centered at some value k_0 that determines the soliton velocity in x representation, and that k_0 is small so that $k_0 a \ll 1$. Then we can use the long-wave approximation in Eq. (15) to obtain

$$E(k) \approx E_0 + \frac{\hbar^2 k^2}{2m^*}, \quad \Omega_q \approx V_a |q|, \quad (41)$$

$$\chi(q) \approx 2i\chi \sqrt{\frac{\hbar}{2M\Omega_q}} qa.$$

Taking into account Eqs. (39)–(41) we can rewrite Eqs. (11) and (12) in the following form:

$$i\hbar \frac{\partial \psi}{\partial t} + \frac{\hbar^2}{2m^*} \frac{\partial^2 \psi}{\partial x^2} - [\Lambda + 2\chi\rho] \psi = \varepsilon F(x), \quad (42)$$

$$\frac{\partial^2 \rho}{\partial t^2} - V_a^2 \frac{\partial^2 \rho}{\partial x^2} = \frac{2\chi a V_a^2}{w} \frac{\partial^2 |\psi(x,t)|^2}{\partial x^2} + \varepsilon f(x), \quad (43)$$

where $\rho(x,t)$ is the chain deformation, $\rho(x,t) = \partial u(x,t)/\partial x$, and

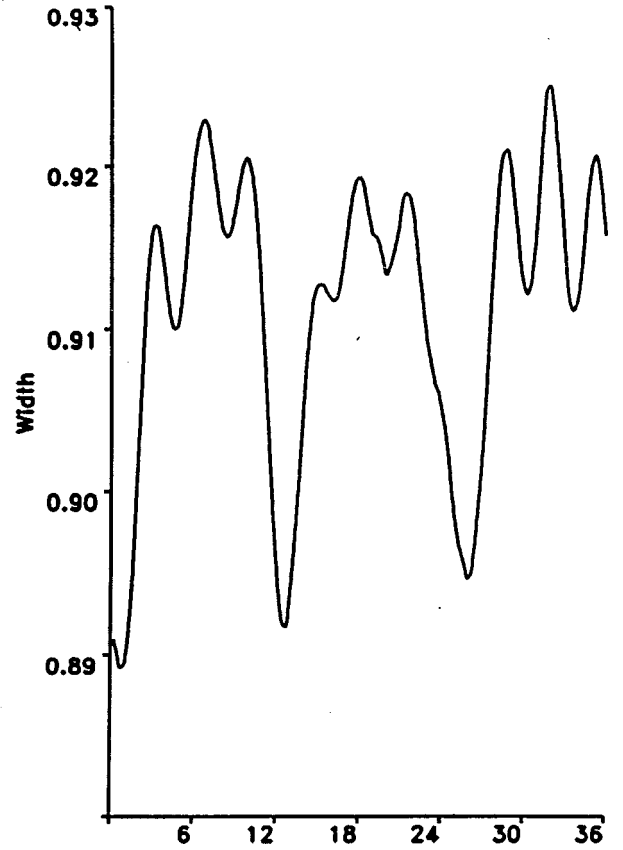


FIG. 12. The width of the soliton as a function of time ($\chi = 90.5$ pN, $l=1$).

$$F(x) = \sum_{n=1,2} [e^{(-1)^n igx} - 1] \frac{1}{L^{3/2}} \sum_{q,k}^{(n)} e^{i(q+k)x} \tilde{\chi}(q) Q_q \Psi_k, \quad (44)$$

$$f(x) = \frac{2\chi V_a c^2}{w} \frac{\partial^2}{\partial x^2} \left[\sum_{n=1,2} [1 - e^{(-1)^n igx}] \right. \\ \left. \times \frac{1}{N} \sum_{k,k'}^{(n)} e^{-i(k'+k)x} \Psi_k^* \Psi_{-k'} + \text{c.c.} \right]. \quad (45)$$

Here $\tilde{\chi}(q) = 2i\chi \sin(qa)$ and the summations in $\sum_{q,k}^{(n)}$, $n=1,2$, are performed in the regions of the Brillouin zone where $q+k > \pi/a$ for $n=1$, and $q+k < -(\pi/a)$ for $n=2$, respectively. Assuming Ψ_k and Q_q are small in these regions, the functions (44) and (45) can be considered as a perturbation.

In the absence of the perturbation, Eqs. (42) and (43) admit the well-known solitonlike solution. The influence of a weak perturbation on the soliton can be accounted for within the adiabatic perturbation theory³⁵ according to which the solution of Eqs. (42) and (43) reads

$$\rho(x,t) = -\frac{2\chi a}{w(1-s^2)} |\psi(x,t)|^2 + \varepsilon \rho_1(x,t), \quad (46)$$

$$\psi(x,t) = \psi_s(x,t) + \varepsilon \psi_1(x,t). \quad (47)$$

Here $\psi_s(x, t)$ is the soliton solution of the nonlinear-Schrödinger equation in the absence of the perturbation

$$\psi_s(x, t) = A \frac{\exp[ik_0(x-r)]}{\cosh[\mu(x-r)]}, \quad (48)$$

with time-depending parameters, namely, the amplitude A , the carrying wave vector k_0 , the soliton center of mass r , and the inverse soliton width μ , which are governed by the following equations:

$$\dot{r} = \frac{\hbar k_0}{m} + \varepsilon \phi_1, \quad \dot{k}_0 = \varepsilon \phi_2, \quad \dot{\mu} = \varepsilon \phi_3, \quad (49)$$

$$\dot{A} = \frac{i}{\hbar} \left(-\Lambda + \frac{\hbar^2 k^2}{2m} + \frac{\hbar^2 \mu^2}{2m} + \varepsilon \phi_4 \right) A, \quad (50)$$

$$\mu^2 = \frac{4m\chi^2 a^2}{\hbar^2 w(1-s^2)} |A|^2 + \varepsilon \phi_5. \quad (51)$$

The quantities ϕ_i are determined by the condition that the correction $\psi_1(x, t)$ in Eq. (47) of the solution of the nonlinear-Schrödinger equation perturbed by the term $\varphi_{pert} = \varepsilon(F + 2\chi\rho_1\psi_s)$ does not contain secular terms.³⁶ This procedure leads to the following equations for functions ϕ_i

$$\phi_1 = -\frac{i}{\hbar} \int_{-L/2}^{L/2} (F\psi_s^* - F^*\psi_s)(x-r) dx, \quad (52)$$

$$\begin{aligned} \phi_2 = & -\frac{\mu}{\hbar} \int_{-L/2}^{L/2} (F\psi_s^* + F^*\psi_s) \tanh[\mu(x-r)] dx \\ & - \frac{4\chi\mu}{\hbar} \int_{-L/2}^{L/2} \rho_1 \tanh[\mu(x-r)] |\psi_s|^2 dx, \end{aligned} \quad (53)$$

$$\phi_3 = \frac{i\mu}{\hbar} \int_{-L/2}^{L/2} (F\psi_s^* - F^*\psi_s) dx, \quad (54)$$

$$\begin{aligned} \phi_4 = & -\mu \int_{-L/2}^{L/2} (F\psi_s^* + F^*\psi_s)(x-r) \tanh[\mu(x-r)] dx \\ & - 4\chi\mu \int_{-L/2}^{L/2} \rho_1 \tanh[\mu(x-r)](x-r) |\psi_s|^2 dx \\ & - ik_0 \int_{-L/2}^{L/2} (F\psi_s^* - F^*\psi_s)(x-r) dx - \frac{\hbar^2}{3m} \phi_5, \end{aligned} \quad (55)$$

$$\phi_5 = \frac{i\mu^2}{\hbar} \int_{-L/2}^{L/2} (F\psi_s^* - F^*\psi_s) dx. \quad (56)$$

Here we will analyze the dynamic equation for the soliton center of mass, $r(t)$, since it represents one of the most important results of the analytical model. According to Eqs. (52) and (53), this equation takes the form

$$m\ddot{r}(t) + \int_0^t \ddot{r}(t-\tau) K(\tau) d\tau = -\frac{\pi}{a} U_P \sin\left(\frac{2\pi r}{a}\right), \quad (57)$$

where

$$K(\tau) = -\frac{4\chi^2 a \mu}{wV_a^2} \frac{d}{d\tau} \frac{\mu V_a \tau \cosh(\mu V_a \tau) - \sinh(\mu V_a \tau)}{\sinh^3(\mu V_a \tau)}, \quad (58)$$

$$U_P = \frac{4\pi^2 J}{\mu a N^2} \sum_{q,k}^{(1)} \frac{(g-q-k)a \sin(qa)}{\sinh\left(\frac{\pi q}{2\mu}\right) \cosh\left[\frac{\pi(k-k_0)}{2\mu}\right] \cosh\left[\frac{\pi(k-k_0+q-g)}{2\mu}\right]}. \quad (59)$$

The kernel $K(\tau)$ (58) is determined by the reaction of the lattice on the soliton acceleration and leads to the effective soliton mass m_s , (38) in the dynamic equation (57) at slow acceleration. The right-hand side term in Eq. (57) indicates that the soliton moves in the periodical (with lattice period) Peierls-Nabarro potential

$$U(r) = U_P \sin^2\left(\frac{\pi r}{a}\right). \quad (60)$$

The soliton motion in a periodical potential has been considered in Ref.³⁷. A soliton can overcome the barrier and move along the chain only if its initial kinetic energy $E_{kin} = m_s V_0^2/2$ exceeds the height of the Peierls-Nabarro barrier, Eq. (60), which is possible when the value of k_0 exceeds the critical value k_{cr} ,

$$k_{cr} = \sqrt{\frac{2m^2 U_P}{\hbar^2 m_s}}. \quad (61)$$

At small values of the initial wave number, i.e., for $k_0 < k_{cr}$, pinning of a soliton by the lattice takes place and the soliton oscillates between the neighboring barriers even if its width exceeds the lattice spacing, as can be seen by the oscillation of soliton c.m.c. shown in Fig. 9. With increasing k_0 , the soliton kinetic energy increases and at $k_0 > k_{cr}$ the soliton can move along the chain.

It should also be noticed that in the general case, according to Eq. (59), the height of the Peierls-Nabarro barrier depends on the width of the soliton and its wave vector. From Eq. (59) at $\mu a < 1$ we find the following estimation of U_P :

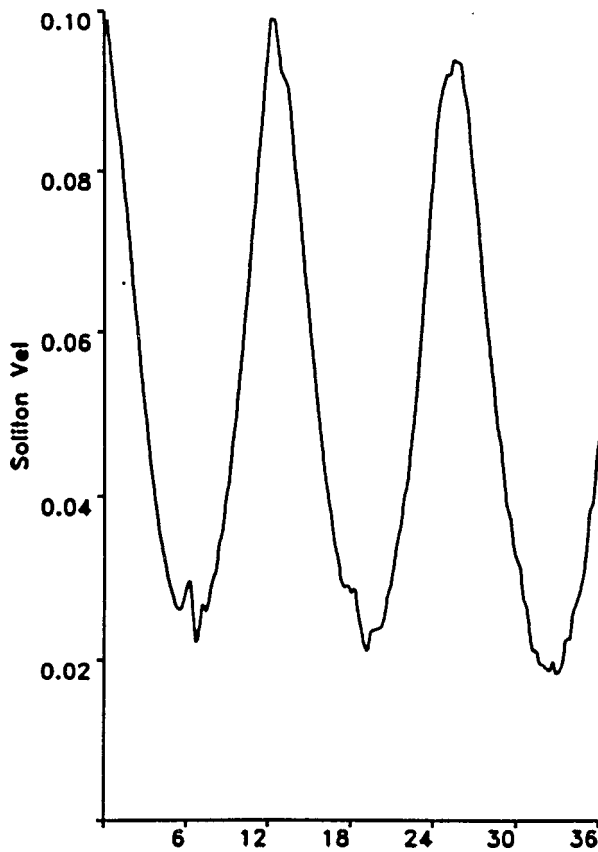


FIG. 13. Soliton velocity as a function of time ($\chi=90.5$ pN, $l=1$).

$$U_p = \frac{4(\pi^2 + 4)J}{\mu a} \exp\left(-\frac{\pi^2}{2\mu a}\right) \left[1 + o\left(\frac{\mu^3}{\pi^3}\right)\right]. \quad (62)$$

Hence, for a broad soliton the critical value k_{cr} (61) is very small and such a soliton moves with a nonzero velocity even at small values of k_0 . Moreover, at values of the wave number k_0 that exceed the critical value, the soliton is still sensitive to the presence of the barrier. The dependence of its velocity, momentum and energy on k_0 differ from those predicted by the continuum models (see, Fig. 10 and Fig. 11). Indeed, instead of a monotonic relation, those variables are oscillating functions of time. From Eq. (57) one can obtain the instantaneous soliton velocity:

$$V(t) \equiv \dot{r}(t) = V_0 dn(u, \kappa) = \bar{V} \left[1 + \sum_{n=1}^{\infty} \frac{4q^n \cos(n\omega t)}{1+q^{2n}}\right], \quad (63)$$

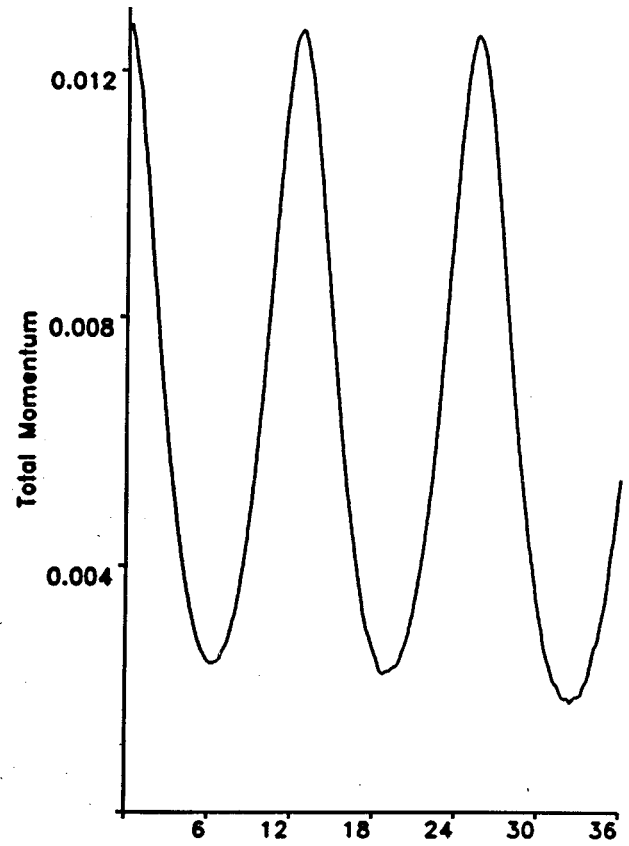


FIG. 14. Soliton momentum as a function of time ($\chi=90.5$ pN, $l=1$).

where $dn(u, \kappa)$ is the Jacobi elliptic function, $u = \pi V_0 t / a$, and $\kappa^2 = U_p / E_{kin}$, is the modulus of the elliptic integral. According to Eq. (63) the soliton moves with an average soliton velocity, $\bar{V} = \pi V_0 / 2K(\kappa)$, and has oscillating components with a main harmonic $\omega = \pi^2 V_0 / 2aK(\kappa)$ and its overtones. Here V_0 is the initial soliton velocity due to the initial wave vector k_0 as given by the relation (25), $K(\kappa)$ is the complete elliptic integral of the first kind, and $q = \exp(-\pi K' / K)$, where $K' = K(\kappa')$, $\kappa'^2 = 1 - \kappa^2$.

From Eqs. (49) and (54) we get the equation for the soliton width

$$\dot{\mu} = -\mathcal{M} \sinh\left(\frac{\pi m V}{2\hbar \mu}\right) \sin\left(\frac{2\pi r}{a}\right), \quad (64)$$

where

$$\mathcal{M} = \frac{2\pi^3 \chi^2}{\hbar L^2 w \mu} \sum_{k,q}^{(1)} \frac{\sin(qa) \sinh\left(\frac{\pi(2k+q-g)}{2\mu}\right)}{\sinh\left(\frac{\pi q}{2\mu}\right) \cosh^2\left(\frac{\pi k}{2\mu}\right) \cosh^2\left(\frac{\pi(k+q-g)}{2\mu}\right)}. \quad (65)$$

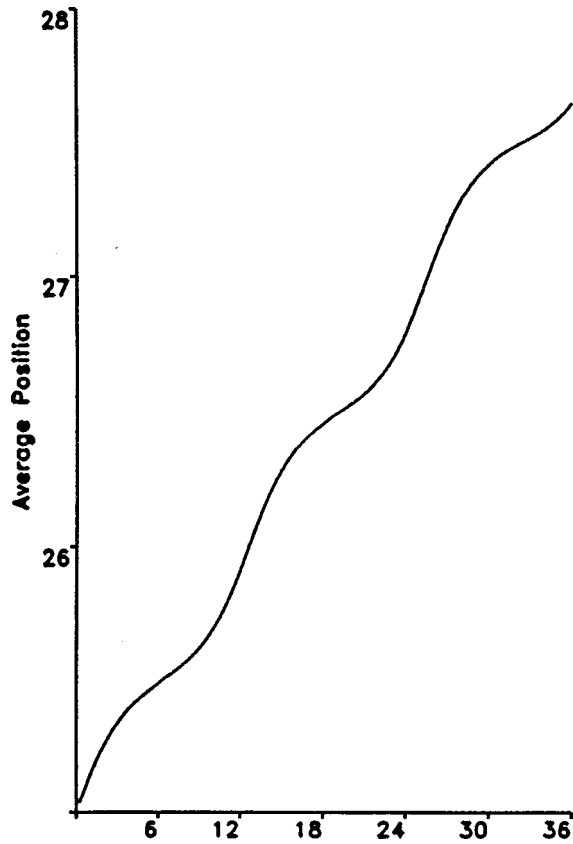


FIG. 15. Soliton c.m.c. as a function of time ($\chi=90.5$ pN, $l=1$).

From Eq. (64) we conclude that the oscillations of the soliton width take place during the soliton propagation through the discrete potential relief. It is difficult to see these oscillations in Fig. 1 since the soliton is spread over few lattice sites, while the oscillations of the soliton amplitude are distinctly seen. And indeed, an amplitude of a soliton and its width are connected by the normalization condition for the wave function and Eq. (51), which give

$$|A|^2 = \frac{\mu}{2} [1 + O(\varepsilon^2)], \quad \mu = \mu_0 + \varepsilon \frac{\phi_5}{\mu_0}. \quad (66)$$

Here μ_0 coincides with the soliton width as given by the continuum approximations [see Eq. (27)]. The time dependence of a soliton amplitude follows from Eqs. (56) and (64), which determine the oscillations of the soliton amplitude at nonzero velocity.

V. CONCLUSIONS

In the previous sections we have reported the results of numerical and analytical studies of a traveling soliton in a discrete lattice with periodic boundary conditions at arbitrary values of the carrying wave vector. For this we implemented the method of the adiabatic increase of the wave vector described in Sec. II, as well as the analytical scheme of accounting for the discreteness within the corresponding continuum models. These studies reveal that in a discrete lattice a soliton moves in a periodical Peierls-Nabarro potential barrier. The overcoming of this barrier has a threshold character not only with respect to the soliton kinetic energy at given

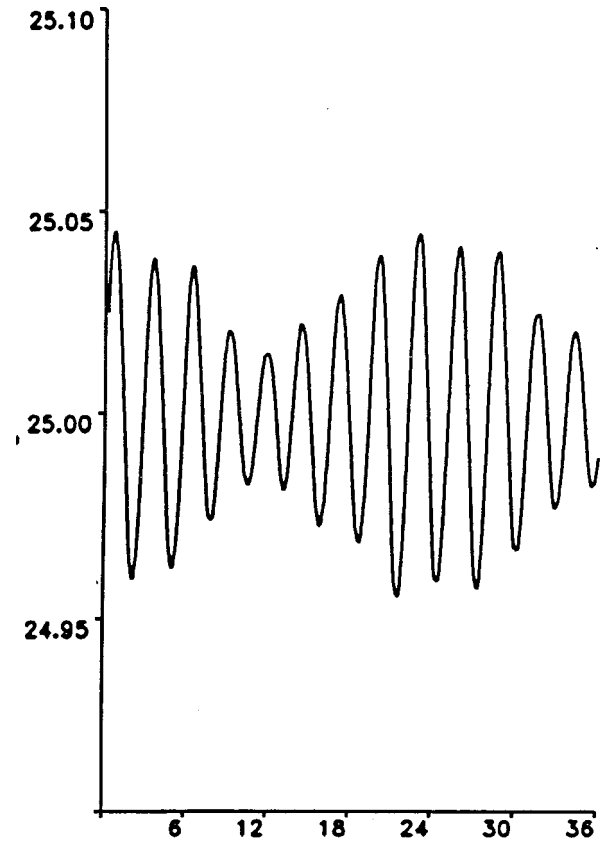


FIG. 16. Soliton c.m.c. as a function of time ($\chi=124$ pN, $l=1$).

values of the soliton parameters, but also with respect to its binding energy as determined by the electron-phonon coupling χ at a given value of the wave number, as is demonstrated in Fig. 9, Fig. 12, and Eq. (61). Similarly, the amplitude of the soliton oscillations within the barrier below the threshold, according to Eqs. (60) and (62), is a function of the value of the carrying wave vector and of the strength of the electron-phonon coupling. This is illustrated in the numerical results displayed in Figs. 13–16.

Due to the lattice discreteness, the soliton velocity contains oscillating terms Eq. (63). Such a soliton center of mass moves with a nonzero instantaneous acceleration \ddot{r} , which results in the emission of sound waves $\rho_1(x,t)$ and, respectively, in soliton deceleration. The motion of the soliton and the sound waves lead to displacements of the molecules from their equilibrium positions and, hence, to the breaking of the initially rigorous periodicity of the lattice. This explains why in the numerical experiments the effect of the potential relief is particularly striking at the very beginning of the soliton motion and becomes less periodic at later times (see Fig. 8) when the periodic potential itself is perturbed by the soliton motion and by the sound waves. This latter effect is a higher-order effect in the perturbation scheme suggested in Sec. IV, but it is automatically accounted for in the numerical simulations of the self-consistent system of Eqs. (17) and (18). Therefore, the properties of solitons in a discrete system and the properties of the Peierls-Nabarro barrier are in mutual connection: on the one hand, the soliton dynamics is influenced by the barrier, and on the other hand, the soliton itself determines this barrier, Eq. (59).

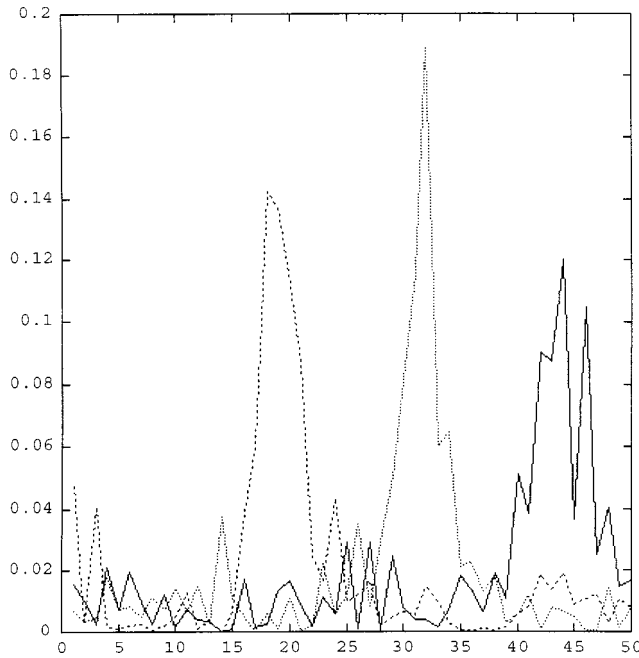


FIG. 17. Amplitude of the soliton envelope as a function of the lattice site n for different times, $\tau=280$ (solid line), 290 (dashed line), and 300 (dotted line) at $l = -14$.

For a broad soliton with $k_0 > k_{cr}$ that moves along the chain with moderate velocity, the Peierls-Nabarro relief is sufficiently shallow. The sound emission and soliton “sonic deceleration” are negligibly small but their roles increase with increasing soliton velocity.

The soliton amplitude in the continuum approximation (20) and (21) increases uniformly with the velocity V because $|A_{sol}|^2 \propto (1-s^2)^{-1}$, $s^2 = V^2/V_a^2$, and its width decreases, $l_{sol} \propto (1-s^2)$. Since $\hbar k_0 = mV$, the amplitude of a soliton in the continuum approximation also increases with k_0 . However, in the numerical simulation this increase of the soliton amplitude and velocity is observed only within some interval of k . At large values of k the velocity reaches a saturation, the value of which depends not only on the sound velocity in the chain, but also on the values of the parameters of electron subsystem.

A further difference with respect to the continuum results is that small oscillations of the soliton width and related to them oscillations of the soliton amplitude take place during soliton propagation along the discrete system, as can be observed in the numerical experiments (see Fig. 1) and as predicted by Eqs. (64) and (66) of the analytical model presented in Sec. IV. It is worth mentioning here that the

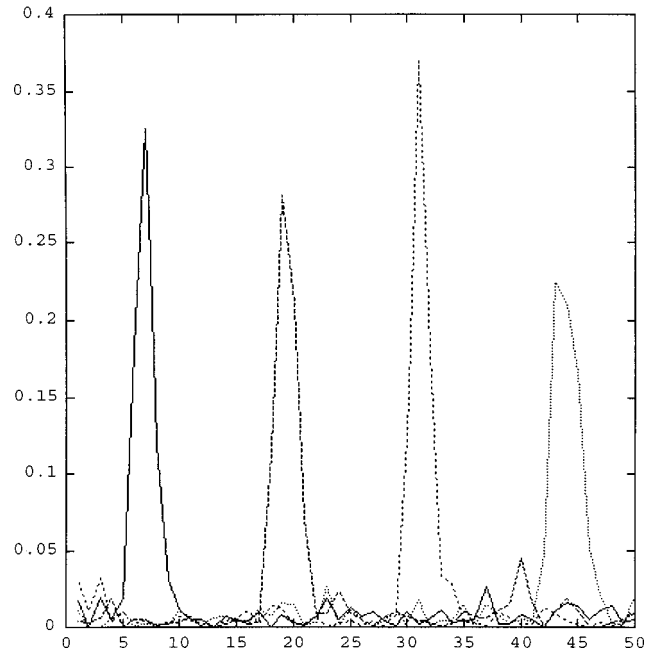


FIG. 18. Amplitude of the soliton envelope as a function of the lattice site n for different times, $\tau=200$ (solid line), 210 (dashed line), 220 (dotted line) at $l = -25$, $w = 9.25$ N/m. The values of the other parameters are the same as in Eq. (37).

oscillations of the soliton amplitude were present in the early numerical calculations on soliton dynamics, e.g., Ref. 7. Also worth mentioning is the asymmetric change of the “leading” and “back” fronts of the soliton envelope due to the motion (see Fig. 5). The oscillations of the soliton amplitude increase with increasing k , which results in the change of the soliton shape. We did not find a shrinking of the soliton into a “small polaron” state localized within one lattice site, due to the soliton motion. At certain parameters of the chain, the increase of k can indeed result in the decay of a soliton, but this is an instantaneous transformation from a smooth one-hump soliton, localized within few lattice sites, into a many-hump and more extended excitation, as shown in Fig. 17. At other values of the parameters, which correspond to the relation $V_{gr} > V_a$, the soliton is stable even for very large values of k (see Fig. 18).

ACKNOWLEDGMENTS

This work was done with support from the Wellcome Trust, Grant No. 048763/Z/96/JMW/JPS, and INTAS Grant, Ref. No. 96-0158.

¹A.S. Davydov and N.I. Kislukha, Phys. Status Solidi B **59**, 465 (1973).

²For Davydov’s soliton, see A.C. Scott, Phys. Rep. **217**, 1 (1992).

³A.S. Davydov, *Solitons in Molecular Systems*, 2nd ed. (Reidel, Dordrecht, 1991).

⁴*Davydov’s Soliton Revisited*, edited by P. L. Christiansen and A. C. Scott (Plenum, New York, 1990).

⁵L. Cruzeiro-Hansson and V.M. Kenkre, Phys. Lett. A **190**, 59 (1994).

⁶A.M. Clogston, H.K. McDowell, P. Tsai, and J. Hanssen, Phys. Rev. E **58**, 6407 (1998).

⁷J.M. Hyman, D.W. McLaughlin, and A.C. Scott, Physica D **3**, 23 (1981).

⁸L. MacNeil and A.C. Scott, Phys. Scr. **29**, 279 (1984) **29**, 284

- (1984).
- ⁹L.S. Brizhik and A.S. Davydov, *Phys. Status Solidi B* **115**, 615 (1983).
- ¹⁰L.S. Brizhik, Yu.B. Gaididei, A.A. Vakhnenko, and V.A. Vakhnenko, *Phys. Status Solidi B* **146**, 179 (1988).
- ¹¹L.S. Brizhik, *Phys. Rev. B* **48**, 3142 (1993).
- ¹²G. Careri, U. Buontempo, F. Galluzzi, A.C. Scott, E. Gratton, and E. Shyamsunder, *Phys. Rev. B* **30**, 4689 (1984).
- ¹³K.J. Donovan and E.G. Wilson, *Philos. Mag. B* **44**, 9 (1981); *J. Phys. C* **18**, 151 (1985).
- ¹⁴A.J. Heeger, S. Kivelson, J.R. Schrieffer, and W.-P. Su, *Rev. Mod. Phys.* **60**, 781 (1988).
- ¹⁵J.L. Brédas, J.C. Scott, K. Yakushi, and G.B. Street, *Phys. Rev. B* **30**, 1023 (1984).
- ¹⁶E.G. Wilson, *J. Phys. C* **16**, 6739 (1983).
- ¹⁷A.A. Gogolin, *Pis'ma Zh. Éksp. Teor. Fiz* **43**, 395 (1986) [*JETP Lett.* **43**, 511 (1996)].
- ¹⁸L.S. Brizhik, A. Eremko, A. La Magna, and R. Pucci, *Phys. Lett. A* **205**, 90 (1995).
- ¹⁹L.S. Brizhik, A. Eremko, and A. La Magna, *Phys. Lett. A* **200**, 213 (1995).
- ²⁰L.S. Brizhik, K. Dichtel, and A.A. Eremko, *J. Supercond.* **12**, 339 (1999).
- ²¹V.V. Kabanov and O.Yu. Mashtakov, *Phys. Rev. B* **47**, 6060 (1993).
- ²²A.S. Alexandrov, V.V. Kabanov, and D.K. Ray, *Phys. Rev. B* **49**, 9915 (1994).
- ²³A.S. Davydov and A.A. Eremko, *Ukr. Fiz. Zh. (Russ. Ed.)* **22**, 881 (1977).
- ²⁴A.A. Eremko, *Spectroscopy of Molecules and Crystals* (Kiev, Naukova Dumka, 1978), pp. 11–17.
- ²⁵W.C. Kerr and P.S. Lomdahl, *Davydov's Soliton Revisited* (Ref. 4), pp. 23–30.
- ²⁶A.S. Davydov and N.I. Kislukha, *Zh. Éksp. Teor. Fiz.* **71**, 1090 (1976) [*Sov. Phys. JETP* **44**, 571 (1976)].
- ²⁷N.I. Kislukha, *Ukr. Fiz. Zh. (Russ. Ed.)* **21**, 829 (1976).
- ²⁸L. Cruzeiro-Hansson, V.A. Okhonin, Khlebopros, and I.N. Yassievich, *Nanobiology* **1**, 395 (1992); L. Cruzeiro-Hansson and V.M. Kenkre, *Phys. Lett. A* **190**, 59 (1994).
- ²⁹A.A. Eremko and A.I. Sergienko, *Fiz. Tverd. Tela (Leningrad)* **24**, 3720 (1982) [*Sov. Phys. Solid State* **24**, 2122 (1982)]; *Ukr. Fiz. Zh. (Russ. Ed.)* **28**, 338 (1983).
- ³⁰R.E. Peierls, *Proc. Phys. Soc. London* **52**, 23 (1940).
- ³¹F.R.N. Nabarro, *Proc. Phys. Soc. London* **59**, 256 (1947).
- ³²V.A. Kuprievich, *Physica D* **14**, 395 (1985).
- ³³A.A. Vakhnenko and Yu.B. Gaididei, *Teor. Mat. Fiz.* **68**, 350 (1986); O.O. Vakhnenko and V.O. Vakhnenko, *Phys. Lett. A* **196**, 307 (1995).
- ³⁴N.J. Ablowitz and J.F. Ladik, *J. Math. Phys.* **17**, 1011 (1976).
- ³⁵A.S. Davydov and A.A. Eremko, *Teor. Mat. Fiz.* **43**, 367 (1980).
- ³⁶J.P. Keener and D.W. McLaughlin, *Phys. Rev. A* **16**, 777 (1977).
- ³⁷A.A. Vakhnenko and A.A. Eremko, *Zh. Tekh. Fiz.* **59**, 1 (1989) [*Sov. Phys. Tech. Phys.* **34**, 1 (1989)].